Microscopic characteristics of the Ag(111)/ZnO(0001) interface present in optical coatings

Zheshuai Lin and Paul D. Bristowe
Department of Materials Science and Metallurgy, University of Cambridge, Cambridge CB2 3QZ, United Kingdom
(Received 13 January 2007; published 16 May 2007)

A first-principles computational method is used to investigate the microscopic properties of the Ag(111)/ZnO(0001) interface that is often present in optical coatings designed for solar-control windows. The mechanical stability of the interface is important and therefore the ideal work of separation has been calculated for several structural variants of the interface which have different lattice mismatches and in-plane orientations. The process by which silver atoms are deposited, cluster, and form layers on the ZnO(0001) surface has also been studied. It is found that interfaces with the O-terminated ZnO surface are stronger than those with the Zn-terminated surface. In addition, incoherent interfaces with small lattice mismatch and minimal strain are preferred. In particular, the large period (9×8) Ag/ZnO coincidence superstructure (0.1% mismatch) is found to have a significantly higher work of separation than the coherent (1×1) interface (11% mismatch). A rotated variant of the interface $(2\times\sqrt{3})$ *R*30 (2.6% mismatch) has a work of separation that is comparable with the coincidence superstructure. Both the (9×8) and $(2\times\sqrt{3})$ *R*30 Ag/ZnO interfaces have been observed in deposition experiments and which one is seen depends on the ambient conditions and strain state of the interface. The calculated works of separation are consistent with measured works of adhesion obtained from cantilever beam experiments.

DOI: 10.1103/PhysRevB.75.205423 PACS number(s): 68.35.−p, 71.15.Nc, 68.35.Np, 68.65.Ac

I. INTRODUCTION

Optical coatings are widely used to block, filter, or reflect light and are typically multilayer structures composed of various oxide films many nanometers thick deposited on a glass or polymer substrate.[1] Each film serves a different purpose, for example, as an antireflective layer, an antiscratch layer, a barrier layer, or a substrate. The deposition process is typically performed using magnetron sputtering[2] since this produces a thin smooth coating using high deposition rates, which is spectrally stable. The layered system that is formed is largely free of defects but, of course, contains many heterophase interfaces which may be strained due to lattice mismatch between the films or diffuse due to chemical mixing. Since the interfaces constitute structural and chemical discontinuities in the system, they will have an important influence on both the optical and mechanical properties of the coating. One specific example is the optical coating designed for solar-control windows which allows visible light to be transmitted but reflects infrared.[3] To achieve this effect, the coating also contains a thin film of low-emissivity metal, usually silver about 10 nm thick, embedded in the system and sandwiched between two of the oxide layers. Below the silver film is usually a ZnO(0001) layer designed to encourage textured growth in the low-energy (111) orientation and above it a barrier layer of indium tin oxide or alumina which protects the silver from damage due to sputtering of further layers above. Mechanical testing of the coating, for example, by scratching or bending has shown that the Ag/ZnO interface is one of the weakest in the multilayer and could deadhere under stress.[4] In addition, since ZnO is hygroscopic, moisture can penetrate the multilayer and this is also known to weaken the interface.[5] It is therefore an important boundary in the system that needs to be characterized at the atomic level and, possibly, modified to improve its properties. The interfacial weakness may be caused by the inherent nature of the metal/oxide bonding, possibly modified by the environmental or thermodynamic conditions present during deposition or afterward while in service. It is thus necessary to understand how silver grows on the oxide substrate and the subsequent structure and chemistry of the interface if better coatings are to be developed, which do not form defects and de-adhere under load. This paper addresses the fundamental properties of the Ag(111)/ZnO(0001) interface using a first-principles computational approach.

To begin a study of the bonding between Ag and ZnO, it is first necessary to specify the structure of the ZnO surface. Zinc oxide, which has the wurtzite structure, is noncentrosymmetric with polar (0001) surfaces. A charge neutral (0001) crystal slab will be terminated by zinc atoms on one face and oxygen atoms on the other. This generates an internal electric field (i.e., dipole moment) perpendicular to the polar surfaces and their electrostatic energy diverges with slab thickness. The stability of this kind of surface, sometimes called "Tasker type-3,"[6] therefore depends on modifying the surface layer geometries or charges.[7–9] In fact, in partial response to the electric fields, ZnO(0001) surfaces relax in practice and develop a complex structure and chemistry that depend on the thermodynamic environment. Experimentally, O-terminated surfaces are reported to be covered with 0.5 ML (monolayer) hydrogen[10] or be (1×3) reconstructed,[11] whereas Zn-terminated surfaces exhibit either a terrace structure with triangular holes and steps or a (2×1) reconstruction covered by OH groups.[12] The partial pressure of oxygen or hydrogen in the ambient atmosphere significantly affects the O or Zn vacancy concentration on ZnO surfaces.[13] In order to perform the density-functional calculations presented here, some simplifying chemical and structural assumptions must be made. Only clean, unreconstructed, defect-free surfaces are considered and used as the substrate onto which the silver is adsorbed. In effect, this implies that the O-terminated surface is formed under O-rich

conditions and the Zn-terminated surface is formed under H-rich conditions. It is important to establish the microscopic characteristics of an ideal interface before the effects of stoichiometry, OH adsorption, water inclusions, and impurities are considered. This will be the subject of future investigations.

There have been several experimental studies on the deposition of silver onto ZnO(0001) surfaces using electron-beam evaporation,[14] magnetron sputtering,[15] and molecular effusion.[16] In the magnetron sputtering experiments, the ZnO is first deposited onto sheet glass, whereas in the other two approaches, the ZnO is a freestanding substrate. In all cases, it is found that the silver films grow in the [111] orientation although two of the studies differ with regard to the growth mode. The electron-beam study[14] concluded that silver grows by a layer-by-layer mode (Frank–van der Merwe mode[17]), whereas the molecular effusion work using a Knudsen cell[16] and the magnetron sputtering experiments concluded that the growth process involves the formation of individual three-dimensional islands (Volmer-Weber mode[18]). The difference in observed growth modes is likely due to the different experimental conditions employed in the studies such as the temperature and the possible presence of contaminants in the vacuum system, which may deactivate unsaturated bonds on the ZnO surface and favor island growth.[14] In addition to the growth mode, there is also some difference in the observed in-plane structure at the interface. The bulk in-plane lattice parameters for the ZnO(0001) and Ag(111) surfaces are 3.25 Å (Ref. 19) and 2.89 Å,[20] respectively, so their mismatch is relatively large, about +11%. Therefore, the formation of a coherent (1×1) Ag/ZnO boundary is expected to be difficult since it would be highly strained with Ag under tension and, indeed, this interface has not been observed. Relaxation of this boundary to form a semicoherent structure containing an array of misfit dislocations is a possibility,[21] but there is no evidence for this in the deposition studies. This may be due to the thickness of the layers deposited (~10 nm for Ag), which may be less than the critical thickness required for dislocation nucleation.[43] However, two other epitaxial orientations, which give smaller lattice mismatches, have been observed. The lattice mismatch between 9 (8) Ag (ZnO) unit cells is very small, less than −0.1%, and would result in an essentially unstrained incoherent interface. X-ray diffraction measurements of the Ag/ZnO boundary grown by molecular effusion[16] have identified the presence of this structure over most of the interface. In this case, a thin film of (111) Ag with almost bulk lattice parameter aligns perfectly over the (0001) ZnO substrate so that $[110]_{Ag}$ is parallel to $[2\bar{1}\bar{1}0]_{ZnO}$. This creates a coincidence superstructure in the boundary plane with a periodicity of about 26 Å. However, over a small fraction of the interface, another orientation is observed in which the Ag film is rotated by 30±3° about [111] with respect to the incoherent interface. This aligns $[110]_{Ag}$ parallel to $[1\bar{1}00]_{ZnO}$ so that 2 ($\sqrt{3}$) Ag (ZnO) unit cells are in coincidence with a periodicity of about 5.78 Å and a lattice mismatch of −2.6%. The silver layer is thus in compression. This second orientation was observed only on "ill-crystallized" parts of the ZnO surface. Although the molecular effusion experiments detected just a small proportion of the $(2\times\sqrt{3})$ $R30$ interfacial structure, this orientation was found to dominate in the magnetron sputtering experiments.[15] Electron-diffraction measurements confirmed the presence of this orientation, although in the paper the ZnO alignment is mislabeled.

Separately, the toughness or work of adhesion of the Ag/ZnO interface has been measured by mechanical testing using a wedge-loaded double-cantilever-beam technique and was found, on average, to be about 1.3 J m^{-2}.[4] The multilayer specimens used in the tests were fabricated by rf magnetron sputtering and contained both Ag/ZnO interfaces and ZnO/Ag interfaces. In the latter case, ZnO is deposited on Ag and this evidently forms a different interface that is found to be approximately twice as tough as the Ag/ZnO interface. Possible reasons for this are discussed briefly below, but the present work focuses on the weaker Ag/ZnO interface. Neither of the interfaces were characterized structurally in the mechanical testing study.

In this work, a density-functional computational approach is used to compare the structure and strength of three variants of the Ag(111)/ZnO(0001) interface: the (1×1) coherent structure, the $(2\times\sqrt{3})$ $R30$ structure, and the (9×8) incoherent structure. The first structure, although not observed experimentally, is chosen as a reference state from which to make the comparisons. All interfaces are simulated in their ideal form, although in practice their relative stability may well be influenced by the prevailing environmental conditions as noted above. Within the supercell approximation, described below, it is straightforward to perform calculations on the first two variants since the model sizes are small, typically less than 50 atoms. However, the (9×8) incoherent structure has a large periodicity, requiring at least 1000 atoms to construct. This is not currently possible within a density-functional framework and therefore an approach has been adopted which simulates the formation of this interface by calculating the properties of single Ag atoms, small clusters, and monolayers adsorbed on the ZnO surface. A number of other coherent structures with smaller periodicities such as 3 (2) Ag (ZnO) and 4 (3) Ag (ZnO) are also calculated as a way of identifying trends in energy as the (9×8) interface is approached with respect to decreasing lattice mismatch. For each of the three structural variants, the strength of the interface is estimated by calculating the work of separation. The density-functional approach is now a well-established method for simulating metal/oxide interfaces.[22–26]

II. COMPUTATIONAL METHOD

In the present first-principles calculations, the plane-wave pseudopotential method[27] based on density-functional theory[28] (DFT) has been used. The CASTEP program[29] is employed to perform the optimized geometries and the electronic structure calculations. Ultrasoft pseudopotentials[30] are used with the 1s, 2s, and 2p electrons for Zn and the 1s electrons for oxygen treated as core electrons. For silver, 4d and 5s electrons are chosen as the valence electrons. A kinetic-energy cutoff of 400 eV ensures energy convergence to less than 0.020 eV/atom, which is sufficiently accurate for

TABLE I. Calculated bulk lattice parameters and surface relaxations of ZnO and Ag compared with experimental data. a and c are the lattice constants, and u is an internal coordinate of the wurtzite structure which determines the relative position of the anion and cation sublattice along the c axis. A surface value that is positive or negative means a movement away from the surface or towards the bulk respectively (Å), and the subscripts refer to double layers numbered from the surface plane (e.g., Zn_1 and O_1 are the Zn and O ions in the outermost double layer).

			Calculated		
			LDA	GGA-PW91	GGA-PBE	Experimental
ZnO	a (Å)		3.184	3.252	3.257	3.250[a]
	c (Å)		5.150	5.252	5.255	5.207
	c/a		1.617	1.615	1.613	1.602
	u		0.3793	0.3792	0.3792	0.3825
Ag	a (Å)		3.997	4.107	4.103	4.086[b]
				Other works	Present work	Experimental
ZnO (0001)	O-terminated surface	O_1		−0.19[c]	−0.26	−0.22±0.05[d]
		Zn_1		+0.06	+0.02	+0.016±0.008
		O_2			−0.02	−0.02±0.04
		Zn_2			−0.01	+0.010±0.007
	Zn-terminated surface	Zn_1		−0.07		
		O_1		+0.07		
Ag (111)				−0.03[e]	−0.00	−0.0[f]

[a]Reference 40.
[b]Reference 41.
[c]Reference 8.
[d]Reference 42.
[e]Reference 34.
[f]Reference 35.

present purposes. Table I, which gives the relaxed structural parameters of bulk ZnO and Ag, shows that the generalized-gradient approximation (GGA) for the exchange-correlation energy is better than the local-density approximation (LDA). Thus GGA using the Perdew, Burke, and Ernzerhof[31] (PBE) functional has been chosen for all the calculations. The initial geometries are optimized by the Broyden, Fletcher, Goldfarb, and Shannon minimizer.[32] The convergence thresholds between optimization cycles for energy change, maximum force, maximum stress, and maximum displacement are set as 10^{-5} eV/atom, 0.03 eV/Å, 0.05 GPa, and 0.001 Å, respectively. The optimization terminates when all of these criteria are satisfied. The interfaces between Ag(111) and ZnO(0001) are constructed using the supercell method, i.e., periodically repeated slabs. If no free surfaces are present in the slab (i.e., no vacuum), then two interfaces are generated in the model. However, these interfaces will not be the same for crystallographic reasons as discussed below. If a vacuum region is included, then a single interface is created, but so also are two surfaces that may cause charge-transfer effects and unwanted electric fields. Both types of model are used in the present study, and although neither of them is ideal, they can, in combination, be used to deduce useful information about the structure and strength of the Ag/ZnO interface. Monkhorst-Pack k-point meshes with a density of at least $(7\times7\times4)$ points in the Brillouin zone of the primitive ZnO unit cell are chosen.[33] For systems with an odd number of electrons, the results have shown that taking energy differences between spin polarized and unpolarized calculations gives basically identical results. The calculations for the ZnO(0001) free surface show that the spacing of the first (0001) double layer is very close to the results of Wander *et al.*[8] Similarly, the calculated relaxation of the topmost interlayer spacing for the Ag(111) surface is negligible, in good agreement with both previous DFT calculations[34] and experimental measurement.[35] The calculated (111) surface energy is 1.04 J m^{-2}, which compares with experimental values of 1.14 J m^{-2} (Ref. 36) and 1.25 J m^{-2} (Ref. 37) taken from polycrystalline samples. A comparison of the present surface calculations with those from other studies is shown in Table I.

III. RESULTS AND DISCUSSION

In order to form a Ag(111)/ZnO(0001) interface, the relative position of the two materials in the interface plane has to be specified. One way of doing this is with respect to the three different high-symmetry adsorption sites on the ZnO(0001) surface, as shown in Fig. 1. Following the definition of Meyer and Marx[26] the (111) silver crystal could be

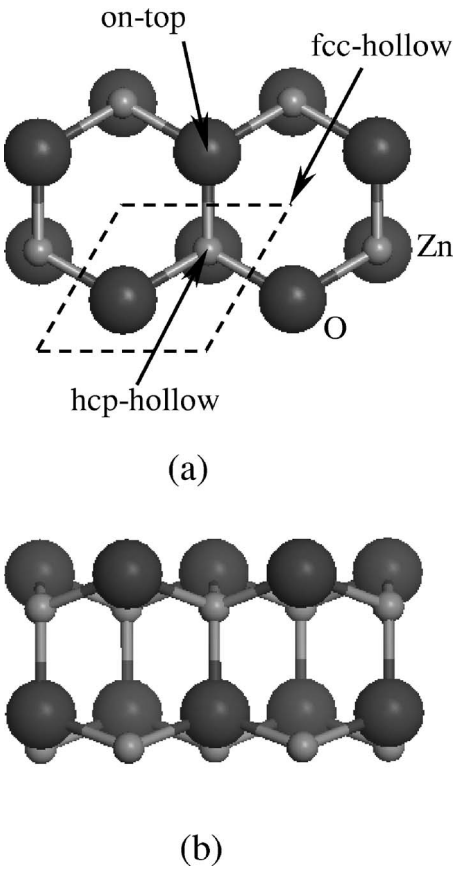

FIG. 1. The O-terminated ZnO(0001) surface. (a) Plan view projected along [0001] with the high-symmetry adsorption sites indicated by arrows and the (1×1) surface unit cell shown by dashed lines. (b) Side view projected along $[10\bar{1}0]$ showing two ZnO(0001) double layers. Large black circles are oxygen atoms.

placed over the ZnO surface with a Ag atom on a "fcc-hollow site," a "hcp-hollow site," or an "on-top site." Given that ZnO is noncentric and has a fourfold stacking sequence $A\alpha B\beta$ along [0001], this would result in 12 distinct interfacial geometries, half of which would be oxygen-terminated (A or B) and the other half zinc-terminated (α or β). However, in the present work, only six of these structures have been considered in detail (e.g., A terminated and β terminated) since the remaining six (B terminated and α terminated) are unlikely to be found during deposition of Ag onto a ZnO(0001) surface. This is because in these cases the ZnO surface is terminated by onefold (dangling) oxygen or zinc atoms that are energetically unfavorable and not observed in practice. The first six translational states (or adsorption sites) of the interface all have Zn (O) terminating atoms that are threefold coordinated and hence more likely to be stable and thus represent the starting structures for optimization. It is noted that all 12 geometries should be considered if interfaces formed from the reverse deposition process are to be studied, i.e., deposition of ZnO onto a Ag(111) surface, since the issue of dangling atoms is not so important. Preliminary calculations have shown that some interfaces in the second set of translational states are significantly more stable than those in the first set, providing support for the experimental observation that there is an asymmetry in the mechanical properties of Ag/ZnO and ZnO/Ag interfaces.[4]

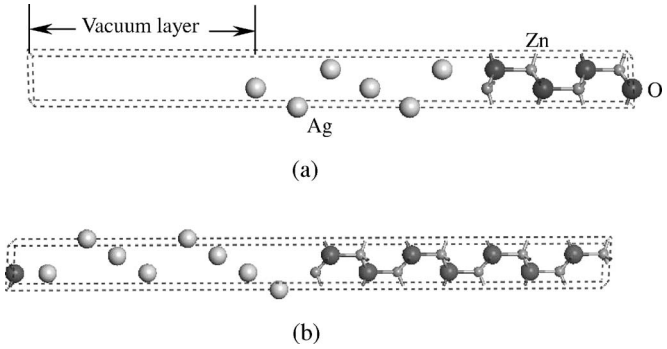

FIG. 2. Schematic of the supercells used to model the (1×1) coherent Ag/ZnO interface. (a) Single-interface model showing the case of a Ag/Zn interface and including a Ag surface and a O surface. (b) Double-interface model with both Ag/Zn and Ag/O interfaces. Smallest gray circles are Zn atoms, large gray circles are Ag atoms, and large black circles are O atoms.

A. Coherent Ag(111)/ZnO(0001) interfaces

1. (1×1) Ag/ZnO interface

Since [0001] is a polar direction in ZnO, it is impossible to construct a supercell containing two identical Ag(111)/ZnO(0001) interfaces. Thus if the properties of an individual translation state of the interface are to be studied, particularly its strength, then a single-interface model is preferred. In the single-interface model a vacuum layer, more than 10 Å thick, is inserted into the supercell [Fig. 2(a)]. This process creates a Ag surface and a Zn (or O) surface as well as an interface, but if the thickness of the vacuum region is chosen to be large enough, then surface-surface interactions can be minimized. Nevertheless, the electronic structure of the interface may still be influenced by electric fields caused by surface dipoles, and therefore, to investigate electronic properties a double-interface model with no vacuum is preferred as discussed below. In the single-interface model, a slab containing four double layers of ZnO and six layers of Ag was chosen. In order to construct the (1×1) coherent interface, the in-plane lattice constant of Ag is increased so that it matches the a lattice constant of ZnO. The Ag lattice is stretched since it requires less energy to do this than compress ZnO. Also, of course, the ZnO represents a thick substrate. Initially, the model is relaxed only with respect to the interlayer spacing at the interface, thus optimizing its local volume. This is called a "volume relaxed" calculation although the in-plane lattice constants remain fixed. Then using the model with optimal interfacial spacing, full atomic relaxation is carried out. In this calculation the atoms around the interface are allowed to move, but the outermost double layer of ZnO and the outermost two layers of Ag are kept rigid. Also the overall supercell dimensions, which include the vacuum region, are held fixed. The single-interface model provides a straightforward and simple way of estimating the strength of individual interfaces within the supercell approximation.

TABLE II. The volume relaxed and fully relaxed interlayer spacings $d_{\text{Ag-O}}$ (or $d_{\text{Zn-Ag}}$) and the ideal works of separation W_{sep} for various interfaces in the single-interface model. Fully relaxed values are shown in parentheses.

	Ag/O interface		Ag/Zn interface	
	$d_{\text{Ag-O}}$ (Å)	W_{sep} (J/m^2)	$d_{\text{Zn-Ag}}$ (Å)	W_{sep} (J/m^2)
On-top	2.21 (2.30)	2.51 (1.40)	2.65 (3.06)	1.12 (0.46)
hcp-hollow	2.08 (2.31)	1.55 (0.74)	2.21 (2.58)	1.49 (0.79)
fcc-hollow	1.92 (2.14)	1.74 (0.83)	2.17 (2.55)	1.46 (0.75)

Table II lists the optimal interlayer spacings and the ideal works of separation for the six Ag/O and Ag/Zn interfaces, with the fully relaxed values given in parentheses. The ideal work of separation is the reversible work that would be needed to cleave an interface if diffusion processes and plastic deformation are suppressed, and is defined by[38]

$$W_{sep} = (E_{slab}^{\text{Ag}} + E_{slab}^{\text{ZnO}} - E_{\text{Ag/ZnO}})/A, \quad (1)$$

where $E_{\text{Ag/ZnO}}$ is the total energy of the supercell with the Ag/ZnO interface present, E_{slab}^{Ag} (E_{slab}^{ZnO}) is the total energy of the same supercell but with the ZnO (Ag) layers replaced by vacuum, and A is the area of the interface. For the volume relaxed calculations, E_{slab}^{Ag} and E_{slab}^{ZnO} are determined from isolated bulk slabs which, in the case of Ag, has been stretched in-plane by 11%. For the fully relaxed calculations, E_{slab}^{Ag} and E_{slab}^{ZnO} are determined from isolated relaxed slabs in which the outermost layers are kept fixed as they are when the interface is present. The ideal work of separation will be a function of model size, particularly the thickness of the Ag crystal, but six Ag layers are found to be enough to allow comparison between different translation states.

The volume relaxed and fully relaxed results in Table II show the same behavior with regard to the strength of the Ag/O and Ag/Zn interfaces. After full relaxation, W_{sep} decreases on average by about 50% and the interlayer spacing increases by about 15%. The increase in interlayer spacing is mainly caused by the Ag layer attempting to recover its bulk volume/atom after relaxation. For the Ag/Zn interface, the hcp-hollow site and the fcc-hollow site have virtually the same work of separation within the accuracy of the calculations and similarly for the Ag/O interface. However, it is clear that the on-top site is the strongest structure for the Ag/O interface but the weakest structure for the Ag/Zn interface. Overall, the Ag/O interface is favored in terms of its strength and stability.

While the single-interface model is suitable for determining interfacial strengths, it may result in inaccuracies when the electronic band structure is calculated due to the presence of an internal electric field and the surface states of ZnO. Consequently, a double-interface model [Fig. 2(b)] with no vacuum region has also been considered despite the fact that it contains different interfaces. This model effectively removes charge-transfer effects due to the vacuum region in the single-interface model, and allows for an independent check on the relaxed structures that were obtained. Relatively thick slabs consisting of eight ZnO double layers are used to eliminate the residual internal electric field,[33] and eight to ten Ag layers are included so that most interface combinations can be considered. All the atom positions and the supercell dimensions are allowed to move during relaxation.

By using the double-interface model, it is necessary to construct nine distinct slab configurations to allow for the presence of all combinations of Ag/O and Ag/Zn interfaces. However, if only the relative strengths of various interfacial combinations are needed, then fewer slabs can be considered. The calculated interlayer spacings and strengths for six combinations are listed in Table III. Here, the strengths refer to the total work needed to separate both interfaces in the model simultaneously. In these calculations, $E_{\text{Ag/ZnO}}$ in Eq. (1) is the total energy of the relaxed supercell containing two interfaces, and E_{slab}^{Ag} and E_{slab}^{ZnO} are the total energies of isolated relaxed slabs obtained from the interface supercell. Since the supercell dimensions are allowed to change during relaxation, the in-plane lattice mismatch is no longer constrained to 11%. Comparison between the interlayer spacings in Tables II and III shows that although the absolute magnitudes are slightly different, the trend is the same, i.e., the Ag/O spacings are smaller than the Ag/Zn spacings. Since the double-interface model is allowed to relax both normal and parallel to the interfaces, some differences are expected. Similarly, it is possible to compare the total work of separation in Table III with the sum of W_{sep} for the corresponding interfaces determined by the single-interface models in Table II. Again the absolute magnitudes are different because of the different boundary conditions imposed in the models but the trend is the same; for example, Ag/O (hcp-hollow) and Ag/Zn (on-top) are the weakest combination of interfaces while Ag/O (on-top) and Ag/Zn (fcc-hollow) are the strongest. Therefore, both types of model are suitable for determining the structural and energetic properties of the Ag/ZnO interface, and the same conclusions can be made. For instance, the silver layer adjacent to the O-terminated interface behaves like the missing next Zn layer, while the silver layer adjacent to the Zn-terminated interface acts like a metal film adsorbed on the Zn layer. Similar adsorption properties have been observed at Cu/ZnO interfaces,[26] except that their interlayer spacings are smaller and their interfacial strengths are stronger. Copper and silver are expected to have similar adsorption characteristics since they belong to the same IB family of elements whose physical properties are dominated by the valence electrons.

Using the double-interface model, the electronic band structures of the most stable interfacial translation states, the on-top site Ag/O interface and the hollow site Ag/Zn interface, have been studied. The electronic properties of the two interfaces are characterized using the layer partial density of states (LPDOS), as shown in Fig. 3. For bulk ZnO (very similar to the LPDOS of ZnO3 in Fig. 3), O 2s orbitals and Zn 3d orbitals are deep in the energy spectrum and have little contribution to the Zn–O bonding. The upper of the valence states (from −8 eV) show a large hybridization between O 2p and Zn 4s orbitals, but the top of the valence band is dominated by O 2p orbitals. The bottom of the conduction band consists mainly of Zn 4s and 4p orbitals. When an ideal

TABLE III. The fully relaxed interlayer spacings and the ideal works of separation for different combinations of interfaces using the double-interface model. $W_{\mathrm{Sep\_d}}^{sum}$ is the combined ideal work of separation resulting from de-adhering both interfaces on opposite sides of the ZnO slab. For comparison, the total work of separation $W_{\mathrm{Sep\_s}}^{sum}$ for the same combination of interfaces derived from the single-interface model is also shown.

	Interfaces		Interlayer spacing (Å)	$W_{\mathrm{Sep\_d}}^{sum}$ (J/m^2)	$W_{\mathrm{Sep\_s}}^{sum}$ (J/m^2)
8ZnO-8Ag1	Ag/O	hcp-hollow	2.00	2.65	1.20
	Ag/Zn	on-top	2.64		
8ZnO-8Ag2	Ag/O	fcc-hollow	1.87	3.48	1.62
	Ag/Zn	hcp-hollow	2.23		
8ZnO-8Ag3	Ag/O	on-top	2.20	4.44	2.15
	Ag/Zn	fcc-hollow	2.22		
8ZnO-10Ag1	Ag/O	on-top	2.19	4.05	1.86
	Ag/Zn	on-top	2.63		
8ZnO-10Ag2	Ag/O	hcp-hollow	2.23	3.12	1.53
	Ag/Zn	hcp-hollow	1.96		
8ZnO-10Ag3	Ag/O	fcc-hollow	1.88	3.36	1.58
	Ag/Zn	fcc-hollow	2.18		

unreconstructed ZnO (0001) surface forms, the upper valence band of the outermost layer contracts since 1/4 of its nearest-neighbor atoms is lost. Moreover, the number of electrons on the Zn atom of the Zn-terminated surface increases since the upper edge of the valence band close to the O-terminated surface is higher than the lower edge of the conduction band at the Zn-terminated surface due to the existence of a dipole moment normal to the interface.[39] The electronic structure of bulk silver (very similar to the LPDOS of Ag3 in Fig. 3) is characterized by 4*d* orbitals located from −8 to −3 eV, and the metallic states are mainly composed of 5*s* and 5*p* orbitals. When an ideal silver (111) surface forms, the valence states of the outermost silver atom also contract.

The presence of Ag/O and Ag/Zn interfaces in the model will modify the electronic structure of the bulk phases and these changes should naturally be concentrated on the layers next to the interface (see LPDOS of Ag1 and ZnO1 layers in Fig. 3). For the Ag/O interface, it is easy to see that there is, in fact, little modification of the LPDOS for the ZnO layers relative to bulk ZnO. This confirms that the adsorption of Ag on the O-terminated ZnO surface replaces the role of Zn on the missing next layer, not only with respect to atomic geometry but also to electronic compensation. At the same time, there is clear indication of hybridization of the Ag 5*s* and 5*p* orbitals with the O 2*p* orbitals in Ag/O interface. For the Ag/Zn interface, the LPDOS of the first double layer of ZnO from the interface shows that the Zn interfacial band states almost keep their shape as in a free Zn-terminated surface. This means that charge transfer from Ag to Zn is very small, the bonding between them preferring to be metallic. The tails of the metallic states become negligible by the second layer from the interface. The adsorption of Ag cannot provide enough electrons to compensate for the charge on the outermost Zn to reproduce its character in bulk ZnO. Charge-density difference maps can also explicitly demonstrate these electronic properties of the interfaces, as shown in Fig. 4. The charge redistribution at an interface is determined by subtracting its valence charge density from that of the free Ag and ZnO separate slabs. For the Ag/O surface, it is clear that a large direction dependent redistribution of charges between Ag and O atoms takes place, whereas for the Ag/Zn interface, the redistribution of charges is much smaller. A similar effect has been found in the Cu/ZnO system.[26] The Ag/Zn interface, therefore, is weaker than the Ag/O interface. For both the Ag/O and Ag/Zn interfaces, the LPDOS on the atoms from the third double layers onward from the interface exhibits little modifications compared to the bulk.

2. $(2 \times \sqrt{3})$ R30 Ag/ZnO interface

The second variant of the Ag/ZnO interface considered involves a 30° rotation of the silver layer about [111] so that $[110]_{\mathrm{Ag}}$ aligns parallel with $[1\bar{1}00]_{\mathrm{ZnO}}$ and, after compressing the silver by 2.6%, creates a coincidence unit cell with a periodicity of about 5.78 Å. Similar to the situation with the (1×1) interface, there are six possible translation states to consider and the three which are O terminated are displayed in unrelaxed form in Fig. 5. Because of the size of the unit cell, only a quarter of the Ag atoms actually occupy the high symmetry sites. Using the single-interface model, the volume relaxed and fully relaxed interlayer spacings at the interface were determined together with the ideal works of separation. The results are given in Table IV, where it is seen that both the spacings and strengths appear to be independent of

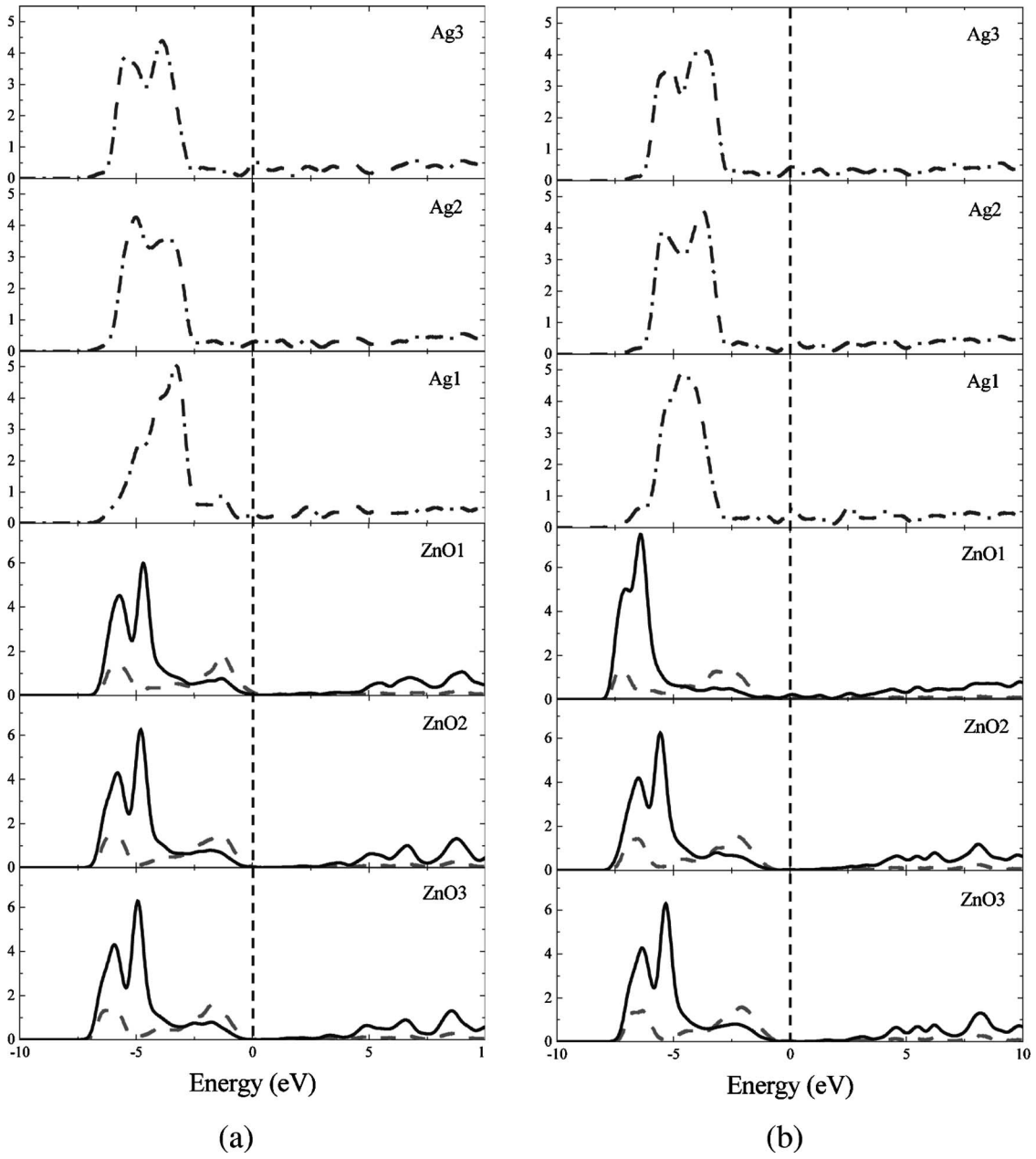

FIG. 3. The layer partial density of states (LPDOS) for (a) the optimal (1×1) Ag/O interface and (b) the optimal (1×1) Ag/Zn interface. The broken vertical lines indicate the Fermi level of silver. The solid, dashed and dashed-dot lines represent the LPDOS on Zn, O, and Ag atoms, respectively. The units are electrons/eV.

translation state for both types of interface. However, as with the (1×1) variant, the Ag/O interface is the strongest and has the smallest interlayer spacings. Thus for this rotated variant of the interface, which has a larger periodicity and smaller lattice mismatch than the (1×1) variant, no specific bonding geometry (i.e., Ag/O translation state) is preferred and its strength is determined by some mean interfacial interaction energy. Compared to the (1×1) interface, the mean ideal work of separation (1.12 J m^{-2}) is clearly smaller than the largest value found for the Ag/O structure (1.40 J m^{-2}) and is therefore weaker than that structure. The largest works of separation for the Ag/Zn structures of both variants are comparable, although the rotated variant is slightly stronger. However, it should be noted that the strain states of the (1×1) and $(2\times\sqrt{3})$ $R30$ interfaces are significantly different (+11% versus −2.6%) and have so far been ignored. The effect of elastic energy on the stability of the interfaces will be considered further below. Calculations using the double-interface model were not performed on the $(2\times\sqrt{3})$ $R30$ interface since, based on the results of the preceding section, no new information was expected.

From the above calculations on both the (1×1) and $(2\times\sqrt{3})$ $R30$ interfaces, it is concluded that Ag adsorption on the Zn-terminated ZnO surface is relatively weak. Therefore, only Ag/O interfaces are considered in the following sections.

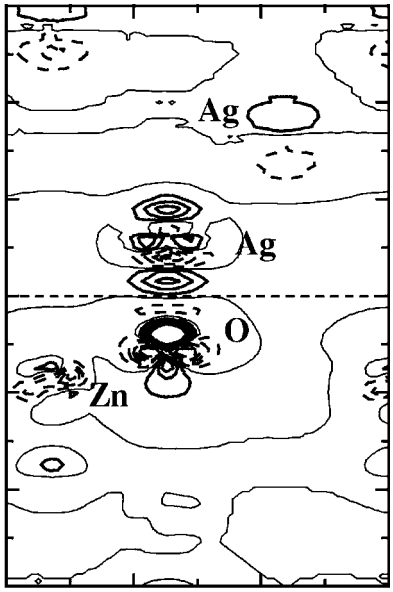

(a)

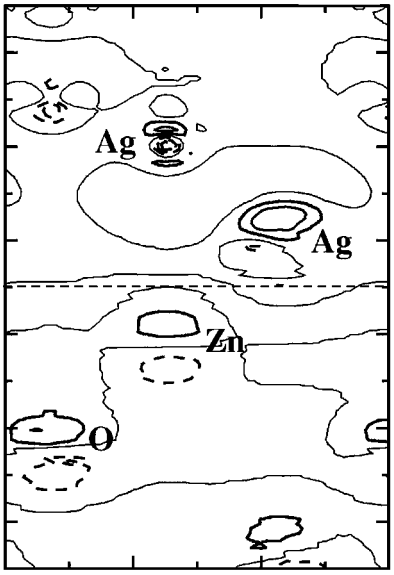

(b)

FIG. 4. Charge-density difference map for (a) the optimal (1×1) Ag/O coherent interface and (b) the optimal (1×1) Ag/Zn coherent interface. Contour intervals are in units of 0.002 e/Å^2. Dashed lines indicate a charge-density reduction.

B. Incoherent (9×8) Ag(111)/ZnO(0001) interface

Since the full (9×8) incoherent interface cannot be relaxed with the present methodology, two different approaches were taken to simulate its structure and strength: firstly, single Ag atoms are added one by one onto an O-terminated (0001) ZnO surface to simulate the initial growth of the large-period structure. Up to 30 Ag atoms in the form of a cluster or monolayer are adsorbed onto the surface, and relaxed bond lengths and adsorption energies are calculated. Secondly, several shorter-period coherent interfaces with large lattice mismatches are studied to determine how their properties vary as the mismatch is reduced toward the −0.1% value of the (9×8) interface. The (9×8) interface is essentially unstrained so the elastic strain energy of the shorter-period interfaces has to be taken into account.

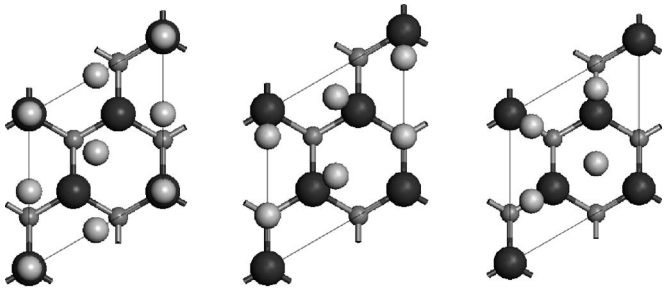

(a) (b) (c)

FIG. 5. The unrelaxed structures viewed along [0001] of three translation states of the $(2\times\sqrt{3})$ $R30$ Ag/ZnO interface with Ag located at (a) the on-top site, (b) the hcp-hollow site, and (c) the fcc-hollow site. Smallest gray circles are zinc atoms and largest black circles are oxygen atoms.

1. Growth of Ag(111) layers on the ZnO(0001) surface

A single-interface model is used in which individual Ag atoms are adsorbed onto an O-terminated ZnO surface and a small cluster or island is grown. The maximum initial area of the Ag cluster on the surface is less than the area of the ZnO slab by two ZnO surface cells, which ensures that the Ag islands are more than 6.5 Å apart due to the periodic boundary condition. The interaction energy between the Ag clusters is calculated to be less than 0.02 eV, so this arrangement is sufficient to describe an isolated Ag cluster. To further improve the accuracy of the calculation, an attempt is made to remove the residual electric field present in the slab due to the polar nature of the oxide, as described in the Introduction. Following the experimental observation[10,12] that hydrogen atoms (H) and hydroxyl ions (OH) are usually adsorbed on the O-terminated and Zn-terminated surfaces, respectively, with 50% coverage, a suitable number of hydroxyl ions are attached to the zinc side of the slab. This changes

TABLE IV. The volume relaxed and fully relaxed interlayer spacings $d_{\text{Ag-O}}$ (or $d_{\text{Zn-Ag}}$) and ideal works of separation W_{sep} for various $(2\times\sqrt{3})$ $R30$ interfaces. Fully relaxed values are given in parentheses.

	Ag/O interface		Ag/Zn interface	
	$d_{\text{Ag-O}}$ (Å)	W_{sep} (J/m^2)	$d_{\text{Zn-Ag}}$ (Å)	W_{sep} (J/m^2)
on-top	2.23 (2.26)	1.70 (1.10)	2.52 (2.49)	1.42 (0.91)
hcp-hollow	2.21 (2.25)	1.72 (1.12)	2.50 (2.52)	1.43 (0.85)
fcc-hollow	2.21 (2.25)	1.73 (1.13)	2.51 (2.52)	1.43 (0.87)

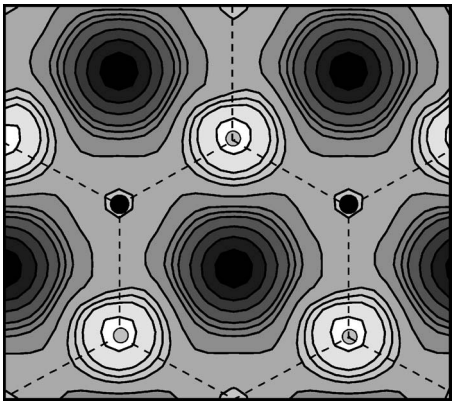

FIG. 6. The energy landscape of a single Ag atom adsorbed on the O-terminated ZnO(0001) surface. The black and gray circles represent O and Zn surface atoms, respectively. The highest (2.1 eV) and lowest (1.5 eV) energy adsorption areas are shown in black and white, respectively. Contour intervals are 0.1 eV. Highest energy adsorption occurs at the fcc-hollow site, whereas lowest energy adsorption occurs at the hcp-hollow site.

the surface charge there from $+2e$ to $+3/2e$, which results in the elimination of the dipole moment as described by Meyer and Marx.[33] [It is not straightforward to apply the same quenching process to a (1×1) slab because of the requirement for 50% coverage. A possible solution is to change the core charge on the hydrogen atom,[26] but this has not been attempted in this study.] A three double-layer ZnO slab is used and Ag atoms are adsorbed on the O-terminated surface. The ZnO interlayer spacings near the surfaces are taken to be the values listed in Table I, and no further relaxation of the slab itself is performed. Tests show that relaxation effects on the surface due to Ag adsorption are about 1%. As the Ag atoms accumulate on the surface, they are assumed to form a cluster having a pyramidal shape. The base layer of the pyramid next to the surface has size $(n\times n)$ Ag atoms, the next layer is $(n-1\times n-1)$, and so on, following the fcc (111) stacking sequence. The largest n used is 4, so in this case the pyramidal cluster has dimensions 16-9-4-1, i.e., 30 atoms. In addition to the interface geometries, the adsorption energy E_{ads} of Ag on ZnO is determined, which is defined as

$$E_{ads} = E_{\mathrm{Ag/ZnO}} - E_{\mathrm{Ag}} - E_{\mathrm{ZnO}}, \tag{2}$$

where $E_{\mathrm{Ag/ZnO}}$, E_{Ag}, and E_{ZnO} are the total energies of the entire system, the Ag atoms, and the ZnO substrate, respectively. The total energies of the Ag atoms are obtained from separate calculations on monolayers and pyramidal clusters of appropriate size. The adsorption energy is considered a more appropriate measure of the strength and stability of the interface between the cluster and the substrate than the work of separation used earlier.

Figure 6 displays the energy landscape of a single Ag atom adsorbed on the O-terminated ZnO(0001) surface. To obtain this landscape, the adsorption energies of a single Ag atom placed at various sites on the substrate are determined. The Ag atom is only allowed to relax normal to the surface. Clearly, for single Ag atom adsorption, the hcp-hollow site is the least stable, the on-top site is next, and the fcc-hollow site is the most favored. This differs from the results described above for the preferred translation state of the (1×1) coherent interface. However, it is analogous to the adsorption of a single Cu atom on the same substrate.[26] The reason is easy to understand; the Ag atom is threefold coordinated to surface oxygen atoms as it is adsorbed at the fcc-hollow site, whereas it is only onefold coordinated at the on-top site. The hcp-hollow site is the weakest due to the presence of metallic bonding with the sublayer Zn atom.

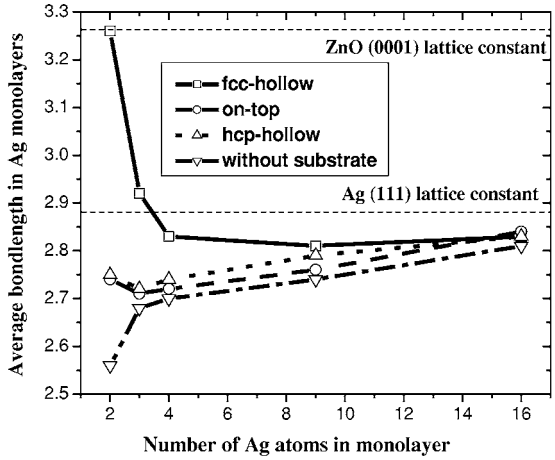

(a)

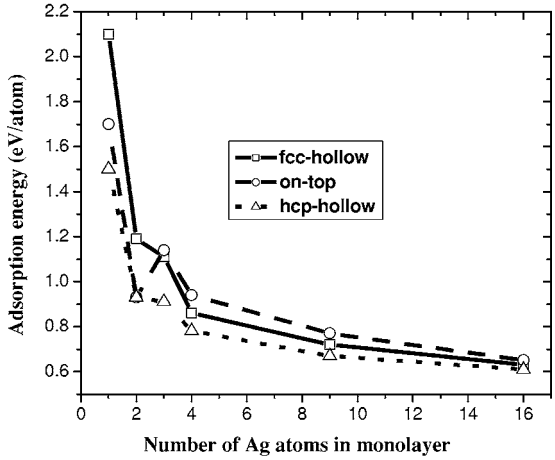

(b)

FIG. 7. The adsorption properties of Ag monolayers initially on the three high-symmetry sites of a ZnO(0001) surface: (a) the average bond lengths and (b) the adsorption energies.

The adsorption properties of further Ag atoms nucleating as monolayers on the three high-symmetry adsorption sites are shown in Fig. 7. The adsorption energy per atom and the average bond length in the monolayer are given. Up to 16 atoms are adsorbed and are allowed to relax away from their starting configurations. In addition, calculations are performed on a corresponding number of Ag atoms without the ZnO slab present to determine its influence on the relaxed Ag bond lengths. These atoms initially lie in a (111) close-packed plane. When two Ag atoms are adsorbed on the sur-

TABLE V. The adsorption properties of four Ag pyramidal clusters adsorbed on the ZnO substrate. The notation, for example, 9-4-1, means that there are nine Ag atoms in the first layer adjacent to the ZnO substrate, four Ag atoms in the second layer, and one Ag atom in the third layer.

Cluster	Initially adsorbed position	E_{ads} (eV/surface atom)	Average $d_{\text{Ag-Ag}}$ in first layer (Å)	Spacing between Ag-ZnO (Å)
3-1	on-top	1.73	2.77	2.18
	fcc-hollow	1.68	2.97	1.93
	hcp-hollow	1.37	2.84	2.21
4-1	on-top	1.71	2.76	2.27
	fcc-hollow	1.66	2.92	2.10
	hcp-hollow	1.35	2.82	2.29
9-4-1	on-top	1.22	2.83	2.29
	fcc-hollow	1.18	2.88	2.23
	hcp-hollow	0.98	2.84	2.30
16-9-4-1	on-top	0.69	2.86	2.27
	fcc-hollow	0.66	2.89	2.25

face, the fcc-hollow sites to which both Ag atoms are strongly bound remain favored. Interestingly, the distance between Ag atoms initially at the on-top (or the hcp-hollow) sites contract to 2.77 Å, much closer to the value without the ZnO substrate (2.56 Å). The most stable adsorption site, however, changes to the on-top site as more Ag atoms are adsorbed and the Ag coordination number increases. At the same time, the hcp-hollow site remains the weakest adsorption site. However, the difference between the adsorption properties for the three high-symmetry sites becomes smaller and smaller with further Ag aggregation; the Ag bond lengths gradually approach the values in bulk and the adsorption energies also converge. A similar situation occurs when the Ag atoms adsorb as a pyramidal cluster instead of a monolayer. Table V gives the adsorption energies, which decrease as the cluster size increases, average bond lengths, and interlayer spacings. These calculated results suggest that when Ag atoms adsorb, cluster, and form films, the interface with ZnO is independent of the initial adsorbed sites. The interface structure and energy depend on the *average* interaction between Ag and ZnO.

The detailed relaxed structures for the Ag monolayer and pyramidal cluster (16 atoms in the first layer) are compared in Fig. 8 as an example. In the monolayer, the bond lengths around the six-coordinated Ag atoms are somewhat different from their bulk value (2.88 Å), and vary from 2.75 to 2.92 Å. At the same time, the monolayer has rumpled, i.e., the central Ag atoms are typically raised off the plane by about 0.2 Å. This implies that the properties of the Ag monolayer partly depend on the adsorption energy landscape of the ZnO(0001) surface. As more Ag atoms adsorb to form the pyramidal cluster, the interaction of the Ag atoms in the upper layers makes the Ag-Ag bond lengths inside the first layer (except the atoms at the edges) almost recover to their bulk values (difference is within 1.5%). Moreover, the rumpling of the first Ag layer has disappeared; it stays flat and the layer spacings inside the Ag cluster almost keep their bulk values (2.37 Å). In addition, with increasing Ag coverage, the interlayer spacings between the ZnO substrate and the adsorbed Ag cluster initially at all three high-symmetry sites gradually approach the same value (the fifth column in Table V). It can be predicted that for the fully incoherent (9×8) interface, which occupies all three high-symmetry sites, the interface spacing is about 2.3 Å.

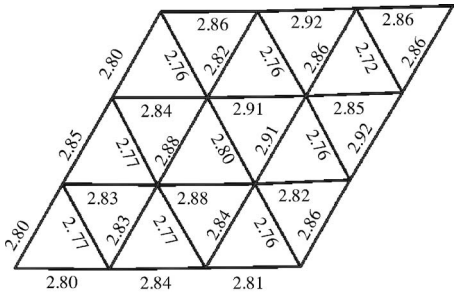

(a)

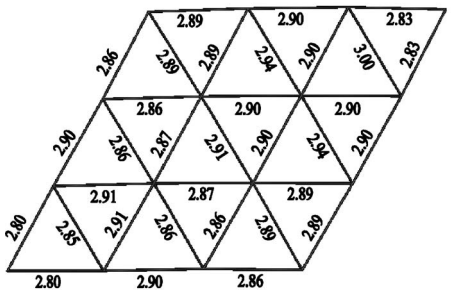

(b)

FIG. 8. The detailed interatomic distances (Å) between 16 Ag atoms constituting the first layer from the Ag/ZnO interface: (a) monolayer and (b) cluster. The Ag atoms are located at the intersections of the lines. Viewed down [0001].

TABLE VI. The total energies (eV) of 4, 9, and 14 Ag atoms adsorbed as a pyramidal cluster on a ZnO substrate compared to the same number of atoms adsorbed as a monolayer. The total energies of the monolayers are set to zero for comparison purposes. A negative energy difference means that the corresponding structure is more stable than the monolayer.

		fcc-hollow	on-top	hcp-hollow
4 atoms	Monolayer	0.0	0.0	0.0
	3-1 cluster	−0.44	−0.32	−0.28
9 atoms	Monolayer	0.0	0.0	0.0
	7-2 cluster	−0.60	−0.57	−0.54
14 atoms	Monolayer	0.0	0.0	0.0
	9-4-1 cluster	−0.93	−0.90	−0.95

TABLE VII. The volume relaxed ideal work of separation W_{sep}, elastic energies E_{el}, and strain-adjusted work of separation W_{Sep}^{adj} for different lattice matched Ag(111)/ZnO(0001) interfaces. The single-interface model is used consisting of two Ag layers and two ZnO double layers.

Interface	Mismatch (%)	E_{el} (J/m^2)	W_{sep} (J/m^2)	W_{Sep}^{adj} (J/m^2)
(3×2)	−33.4	44.46	0.80	−43.66
(4×3)	−18.6	7.16	0.86	−6.30
(5×4)	−11.2	1.64	1.05	−0.59
(6×5)	−6.7	0.22	1.15	0.93
(7×6)	−3.7	0.06	1.19	1.13
(2×$\sqrt{3}$) *R*30	−2.6	0.03	1.14	1.11
(1×1)	+11.1	1.07	1.72	0.65

From the above calculations, it may be concluded that the bonding across the metal/oxide interface is relatively weak compared to the Ag-Ag interaction in the overlayer. This interaction becomes dominant as more Ag atoms aggregate on the O-terminated surface. The Ag/ZnO interface is more likely to be a fully incoherent unstrained nine (eight) Ag (ZnO) interface rather than a relaxed semicoherent interface, even for the first Ag layer from the interface. In fact, for Ag adsorbed on the Zn-terminated surface, the same conclusion may be reached since the strength of the Zn/Ag interface is weaker than that of the Ag/O interface. These conclusions are consistent with the molecular effusion experiments,[16] in which bulklike Ag islands are observed on the (0001) ZnO surface even from the very first stages of growth (~0.17 ML).

The energy of an adsorbed atom in a monolayer can be compared with that of an atom in a three-dimensional cluster to assess which growth mode might be preferred. The results are listed in Table VI. In all cases, the total energies of the Ag clusters are lower than that of the corresponding monolayers with the same number of atoms. This suggests that three-dimensional (3D) island growth might be the preferred growth mode of Ag on the ideal defect-free ZnO(0001) oxygen-terminated surface. This is consistent with some deposition observations[15,16] but not others.[14] However, it is noted that, in practice, the growth process is strongly dependent on the ambient conditions, for example, the growth temperature and the concentration of defects/impurities on the substrate. To fully determine which growth mode is favorable, the kinetics of Ag diffusion on the ZnO surface would need to be simulated using molecular dynamics.

2. Other coherent structures related to the (9×8) Ag(111)/ZnO(0001) interface and the effect of strain energy

Although the full (9×8) incoherent interface cannot be relaxed directly, its relative strength and stability can be estimated by performing calculations on a series of smaller period structures. The periodicities of these interfaces and their corresponding lattice mismatches are given by (7×6) [−3.7%], (6×5) [−6.7%], (5×4) [−11.2%], (4×3) [−18.6%], and (3×2) [−33.4%]. It is seen that the compressive strain which is assumed to be present in the Ag lattice increases as the periodicity decreases. The calculations are performed using the single-interface model, and to further simplify matters, the slab size is reduced to two double ZnO layers together with two Ag layers, and only the interlayer spacing between the two materials is optimized. All the interfaces are O terminated and initially in the on-top position. However, the translation state becomes less important as the periodicity of the interface increases. Although the small model size certainly results in an underestimation of the ideal work of separation, tests have shown that the percentage error is roughly constant across the series. Table VII gives the calculated W_{sep} for the series using this model together with the values for the (1×1) and (2×$\sqrt{3}$) *R*30 interfaces under the same conditions. It is seen that the (1×1) interface has the largest ideal work of separation. However, the values should be adjusted to account for the elastic strain energy present in the Ag lattice, which is different for each interface. To estimate this strain energy, separate calculations are performed on (111) silver slabs, two layers thick, which are relaxed to their bulk geometries. These energies are listed in Table VII and then subtracted from the original work of separation. The strain-adjusted work of separation W_{Sep}^{adj} now shows that the (1×1) interface has a significantly reduced strength and that some interfaces have a negative W_{Sep}^{adj}, indicating that they are intrinsically unstable. The interface with the largest W_{sep}^{adj} is now the (7×6) interface, which has only a 3.7% lattice mismatch. The values are plotted in Fig. 9, where it is seen that an interface with zero lattice mismatch (i.e., unstrained) would have an ideal work of separation of about 1.26 J m^{-2}, corresponding to a maximum on the curve. This interface would be very similar to the (9×8) interface of current interest. Another nearby interface with small strain (8×7) [−1.4%] is estimated to have a work of separation of 1.22 J m^{-2}. Thus it is concluded from these estimates that the large-period unstrained (9×8) structure is the most stable of all the structures considered, but that the (2×$\sqrt{3}$) *R*30, (8×7), and (7×6) structures are also all relatively stable with works of separation that are no more than 10% lower than the (9×8) structure. Thus under the appropriate strain state condi-

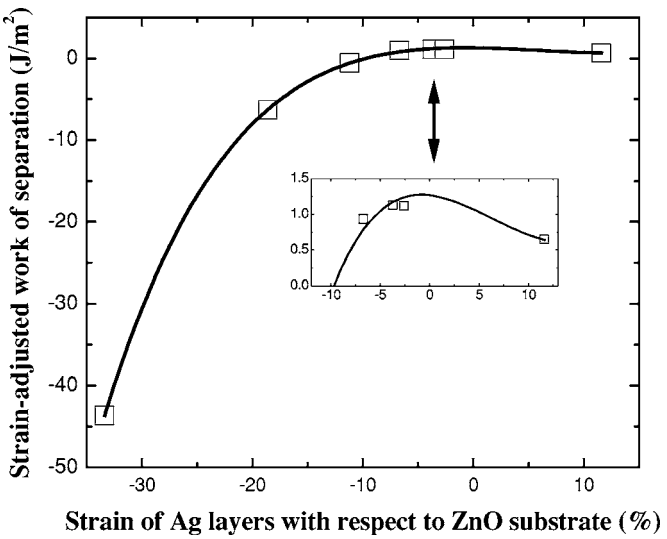

FIG. 9. The strain-adjusted ideal work of separation for various Ag(111)/ZnO(0001) interfaces with different lattice mismatches including the (1×1) and $(2\times\sqrt{3})R30$ variants. The inset shows an enlarged view near zero strain in the Ag layers. The maximum in the curve corresponds approximately to the unstrained (9×8) structure, which is predicted to have a work of separation of 1.26 J/m^2.

tions possibly created by the deposition environment, any of these structures could be found or even coexist. The calculated works of separation for the most stable interfaces are all consistent with the measured works of adhesion, which fall in the range 1.0–1.6 J m^{-2}.[4] Note, however, that the ideal work of separation is thermodynamically different from the work of adhesion and therefore the comparison is only qualitative.[38]

IV. CONCLUSIONS

Using a first-principles computational method based on density-functional theory, the microscopic properties of the defect-free interface between crystals of (111) Ag and (0001) ZnO have been studied. The work has focused on the effect of lattice mismatch and strain energy on the relative strength and stability of several structural variants of the interface. Three different approaches have been used to gain information about the interfaces: a single-interface model in which the mechanical properties of an individual interface formed from two joined crystals can be studied; a double-interface model in which two different interfaces are optimized simultaneously but allows for their electronic structures to be determined; and an adatom model in which the properties of small clusters of atoms on a surface can be studied in an attempt to simulate the initial growth stage of a long-period incoherent interface. For the coherent (1×1) interface, the translation state (or adsorption site) strongly influences the work of separation with the on-top site being preferred for the Ag/O structure and the hcp-hollow site being preferred for the Ag/Zn structure. However, for interfaces with smaller lattice mismatches and larger periodicities, the translational state becomes less important as is found for the $(2\times\sqrt{3})$ $R30$ variant. Even though there is less dependency on the translation state, the O-terminated structure is still stronger than the Zn-terminated structure. Simulations of the initial growth stage of a Ag cluster or monolayer on ZnO confirm the effect of translation state and also reveal the relative strengths of the bonds across the interface and within the growing Ag overlayer. Although the first Ag atom adsorbed prefers the fcc-hollow site, subsequent adsorption shifts the location to the on-top site. As the size of the cluster increases, however, all three high-symmetry adsorption sites become occupied and, moreover, the bond lengths within the Ag material become bulklike. Thus as the Ag film grows, it is predicted to form an unstrained structure, leading to a long-period interface with small lattice mismatch similar to the (9×8) variant. This suggests that the Ag–Ag bonding among layers in the thin film is somewhat stronger than the Ag–ZnO bonding across the interface. A comparison between the total energies of the Ag/ZnO cluster geometries and the monolayer geometries suggests that the unstrained interfacial structure would form via a 3D island growth mode although the kinetics of the processes have not been investigated.

The strain-adjusted ideal works of separation of a series of incoherent interfaces with different lattice mismatches showed that the unstrained (9×8) variant is the strongest but that other structures with small mismatches including the $(2\times\sqrt{3})$ $R30$ variant are also relatively stable. The variant which is observed in practice may depend on the local strain state at the interface which may not be zero due to the presence of point defects, steps, impurities, and water inclusions as mentioned in the Introduction. This may explain the observation of both the (9×8) and $(2\times\sqrt{3})$ $R30$ variants of the Ag(111)/ZnO(0001) interface under different experimental conditions. The conditions prevalent in magnetron sputtering experiments used to fabricate optical coatings appear to favor the $(2\times\sqrt{3})$ $R30$ variant which, because it is more highly strained, may indicate that the ZnO(0001) surface contains defects. In addition, it is known that sputtered ZnO multilayers contain residual stresses of the order of 1 GPa due to the presence of the glass substrate. The effects of these stresses and surface defects on the interfacial properties are currently under investigation.

ACKNOWLEDGMENTS

This work was carried out within Materials Modelling Consortium on Functional Coatings funded by the EPSRC. The calculations were performed using the CCHPCF computing facilities at the University of Cambridge and the HPCx computing facilities at the Daresbury Laboratory. The authors are grateful to John Ridealgh, Paul Warren, and Monica Hughes for useful discussions.

[1] *Handbook of Optical Properties: Thin Films for Optical Coatings*, edited by R. E. Hummel and K. H. Guenther (CRC, Boca Raton, FL, 1995), Vol. 1.
[2] P. J. Kelly and R. D. Arnell, Vacuum **56**, 159 (2000).
[3] H. J. Glaser, *Large Area Glass Coating* (Von Ardenne Anlagentechnik, Gmbh, 2000).
[4] E. Barthel, O. Kerjan, P. Naela, and N. Nadaud, Thin Solid Films **473**, 272 (2005).
[5] E. Ando and M. Miyazaki, Thin Solid Films **251**, 308 (1999).
[6] P. W. Tasker, J. Phys. C **12**, 4977 (1979).
[7] C. Noguea, J. Phys.: Condens. Matter **12**, R367 (2000).
[8] A. Wander, F. Schedin, P. Steadman, A. Norris, R. McGrath, T. S. Turner, G. Thornton, and N. M. Harrison, Phys. Rev. Lett. **86**, 3811 (2001).
[9] A. Wander and N. M. Harrison, J. Chem. Phys. **115**, 2312 (2001).
[10] V. Staemmler, K. Fink, B. Meyer, D. Marx, M. Kunat, S. G. Girol, U. Burghaus, and C. Woll, Phys. Rev. Lett. **90**, 106102 (2003).
[11] M. Kunat, S. G. Girol, T. Becker, U. Burghaus, and C. Woll, Phys. Rev. B **66**, 081402(R) (2002).
[12] O. Dulub, U. Diebold, and G. Kresse, Phys. Rev. Lett. **90**, 016102 (2003); G. Kresse, O. Dulub, and U. Diebold, Phys. Rev. B **68**, 245409 (2003).
[13] B. Meyer, Phys. Rev. B **69**, 045416 (2004).
[14] W. Gaebler, K. Jacobi, and W. Ranke, Surf. Sci. **75**, 355 (1978).
[15] M. Arbab, Thin Solid Films **381**, 15 (2001).
[16] N. Jedrecy, G. Renaud, R. Lazzari, and J. Jupille, Phys. Rev. B **72**, 045430 (2005); **72**, 195404 (2005).
[17] F. C. Frank and J. H. Van der Merve, Proc. R. Soc. London, Ser. A **198**, 205 (1949).
[18] M. Volmer and A. Weber, Z. Phys. Chem., Stoechiom. Verwandtschaftsl. **119**, 277 (1926).
[19] Y. N. Xu and W. Y. Ching, Phys. Rev. B **48**, 4335 (1993).
[20] A. Smakula and J. Kalnajs, Phys. Rev. **99**, 1737 (1955).
[21] W. P. Vellinga and J. Th. M. de Hosson, Acta Mater. **45**, 933 (1997).
[22] C. Kruse, M. W. Finnis, J. S. Lin, M. C. Payne, V. Y. Milman, A. de Vita, and M. J. Gillan, Philos. Mag. Lett. **73**, 377 (1996).
[23] T. Ochs and C. Elsasser, Z. Metallkd. **93**, 406 (2002).
[24] A. E. Mattsson and D. R. Jennison, Surf. Sci. **520**, L611 (2002).
[25] R. Benedek, A. Alavi, D. N. Seidman, L. H. Yang, D. A. Muller, and C. Woodward, Phys. Rev. Lett. **84**, 3362 (2000).
[26] B. Meyer and D. Marx, Phys. Rev. B **69**, 235420 (2004).
[27] M. C. Payne, M. P. Teter, D. C. Allan, T. A. Arias, and J. D. Joannopoulos, Rev. Mod. Phys. **64**, 1045 (1992).
[28] P. Hohenberg and W. Kohn, Phys. Rev. **136**, B864 (1964).
[29] M. D. Segall, P. J. D. Lindan, M. J. Probert, C. J. Pickard, P. J. Hasnip, S. J. Clark, and M. C. Payne, J. Phys.: Condens. Matter **14**, 2717 (2002).
[30] D. Vanderbilt, Phys. Rev. B **41**, 7892 (1990).
[31] J. P. Perdew, K. Burke, and M. Ernzerhof, Phys. Rev. Lett. **77**, 3865 (1996).
[32] T. H. Fischer and J. Almlof, J. Phys. Chem. **96**, 9768 (1992).
[33] B. Meyer and D. Marx, Phys. Rev. B **67**, 035403 (2003).
[34] N. H. de Leeuw and C. J. Nelson, J. Phys. Chem. **107**, 3528 (2003).
[35] F. Jona and P. M. Marcus, in *The Structure of Surfaces II*, edited by J. F. Van der Veen and M. A. Van Hove (Springer-Verlag, Heidelberg, 1988), p. 90.
[36] D. McLean, *Grain Boundaries in Metals* (Oxford University Press, Oxford, 1957).
[37] H. L. Skriver and N. M. Rosengaard, Phys. Rev. B **46**, 7157 (1992).
[38] M. W. Finnis, J. Phys.: Condens. Matter **8**, 5811 (1996).
[39] I. Ivanov and J. Pollmann, Phys. Rev. B **24**, 7275 (1981).
[40] E. H. Kisi and M. M. Elcombe, Acta Crystallogr., Sect. C: Cryst. Struct. Commun. **45**, 1867 (1989).
[41] M. E. Straumanis and S. M. Riad, J. Mater. Sci. **23**, 757 (1988).
[42] N. Jedrecy, M. Sauvage-Simkin, and R. Pinchaux, Appl. Surf. Sci. **162-163**, 69 (2000).
[43] J. W. Matthews and A. E. Blakeslee, J. Cryst. Growth **27**, 118 (1974).